Supporting Information

Davare et al. 10.1073/pnas.1319583110

SI Methods

In Vivo Inhibitor Treatment of Tumor-Bearing Mice. All animal experiments were performed in accordance with a protocol approved by the Memorial Sloan-Kettering Institutional Animal Care and Use Committee. Foretinib was dissolved in DMSO, aliquoted, and stored at −80 °C. Before use, aliquots were further diluted in 1% hydroxypropylmethylcellulose/0.2% SDS. Crizotinib was reconstituted in 1% hydroxypropylmethylcellulose/0.2% SDS, aliquoted, and stored at −80 °C. Tumor cell lines expressing either the FIG–ROS kinase fusion or shRNA against murine phosphatase and tensin homolog (Pten) were s.c. injected into 11-wk-old female immunodeficient Crl:Nu-*Foxn1*^{nu} mice weighing 26 g. Upon reaching a tumor diameter of 4–6 mm, mice were treated with foretinib (25 mg/kg; molecular weight = 632.65), crizotinib (25 mg/kg; molecular weight = 450.34), or vehicle control by oral gavage once daily for 9 consecutive days. Caliper measurements were taken at the time of treatment initiation (T_0) and at 24 h after administration of the last dose (T_{end}). Data in the waterfall plots are calculated as follows: ((tumor volume T_{end}/tumor volume T_0) − 1). Tumor volume is calculated as: $0.5 \times L \times W^2$ with $L > W$.

Isolation of Primary Liver Progenitor Cells and Tumor Cell Line Generation. A detailed description of the production and characterization of cholangiocarcinomas from these cells are described in the companion paper in PNAS (1). Isolation of liver progenitor cells was performed as previously described (2). Briefly, to produce tumors, hepatoblasts of the genotype AlbCre$^{+/-}$; lsl Kras$^{G12D+/-}$; p53$^{R172H/loxp}$ were isolated from embryonic day (ED) 14.5 mouse embryos and retrovirally transduced with either the FIG–ROS fusion or a potent short hairpin RNA against Pten (shPten.1522). At 48 h post transduction, 1×10^6 cells were resuspended in 25 μL Matrigel (BD) and injected subcapsular into the livers of immunodeficient (Crl:Nu-*Foxn1*^{nu}) nude mice. Upon tumor formation, tumors were explanted and subjected to collagenase digestion (Sigma; C1538). Crude digests were plated onto gelatin-coated plates. Enrichment of tumor cells was enhanced by differential trypsinization or cell sorting. These murine cholangiocarcinoma tumor-derived cell lines expressing FIG–ROS (lines 3 and 4) and shPten (lines 1 and 2) were further cultured and maintained in DMEM-high glucose medium (Invitrogen) supplemented with 10% FCS (Invitrogen), L-glutamine (Invitrogen), and penicillin/streptomycin (Invitrogen).

Plasmid Construction. The FIG–ROS–S fusion gene was synthesized using the GeneArt service (Invitrogen). FIG–ROS–S is denoted as FIG–ROS here. FIG–ROS was further subcloned into the retroviral vector, pMSCV–IRES–GFP (pMIG) using the Gateway Cloning system (Invitrogen). SLC–ROS–S (SLC–ROS) was cloned from cDNA made from the non-small cell lung cancer cell line, HCC78. Briefly, using sense primers that were SLC34A2 N-terminus specific (5′ CAC CAT GGC TCC CTG GCC TGA ATT GG) and anti-sense primers that are ROS1-specific (5′ TTA ATC AGA CCC ATC TCC ATA TCC ACT GTG AGT G), we were able to amplify both SLC–ROS–L and SLC–ROS–S from HCC78 cDNA. We individually cloned SLC–ROS–L and SLC–ROS–S after gel extraction of the PCR products into the Gateway Cloning system compatible entry vector pENTR–D/TOPO (Invitrogen) and further subcloned into the pMIG retroviral vector as described above. The FIG–ROS point mutations were created using the Quikchange site-directed mutagenesis kit (Agilent Technologies) according to the manufacturer's protocol.

IL-3 Withdrawal/Transformation Assays. Parental Ba/F3, pMIG-alone, FIG–ROS (wild-type or ROS1 KD mutant variants) or SLC–ROS-expressing Ba/F3 cells (3×10^6 cells total) were washed three times with 50 mL of RPMI-10% FBS media and resuspended in a new 6 mL of RPMI-10% FBS media. The total number of viable cells was counted every other day using Guava ViaCount reagent and a Guava Personal Cell Analysis flow cytometer (Guava Technologies). If cells grew to cell densities $>1.5 \times 10^6$/mL in withdrawal media, the cells were centrifuged and resuspended in fresh media to keep a final culture density of 0.5×10^6/mL.

Immunoblotting. Ba/F3 FIG–ROS, SLC–ROS, HCC78, and murine cholangiocarcinoma cell lines were treated with the indicated concentrations of inhibitors for 1–2 h. In the case of Ba/F3 cells, after treatment 5×10^6 cells were pelleted, washed once in ice-cold PBS, and lysed in 200 μL of cell lysis buffer (Cell Signaling Technology) supplemented with 0.25% deoxycholate, 0.05% SDS, and protease and phosphatase inhibitors. After protein quantification, equal amounts of protein containing lysate were either used for immunoprecipitation where indicated or extracted with SDS sample buffer for 15 min at 80 °C. Proteins were transferred to Immobilon-FL membranes (Millipore) and subjected to immunoblot analysis with antibodies specific for phospho-ROS1 [Cell Signaling Technology (CST); 3078], total ROS1 (CST; 3266), phospho-SHP2 (CST; 3751), total SHP2 (CST; 3752), phospho-STAT3 (CST; 9145), total STAT3 (CST; 4904), phospho-ERK1/2 (CST; 9101), total ERK2 (Santa Cruz; sc-1647), phospho-S6 (CST; 4858), total S6 (CST; 2216), phospho-SRC (CST; 2105), total SRC (CST; 2110), α-tubulin (Sigma; T6199), and β-actin (Sigma; A1978). We used the LI-COR Odyssey imaging system or the Bio-Rad Chemidoc imaging station and followed the manufacturer's protocol for immunoblot detection with use of IR dye or HRP-conjugated secondary antibodies, respectively.

1. Saborowski A, et al. (2013) Mouse model of intrahepatic cholangiocarcinoma validates FIG–ROS as a potent fusion oncogene and therapeutic target. *Proc Natl Acad Sci USA*, 10.1073/pnas.1311707110.

2. Zender L, et al. (2005) Generation and analysis of genetically defined liver carcinomas derived from bipotential liver progenitors. *Cold Spring Harb Symp Quant Biol* 70: 251–261.

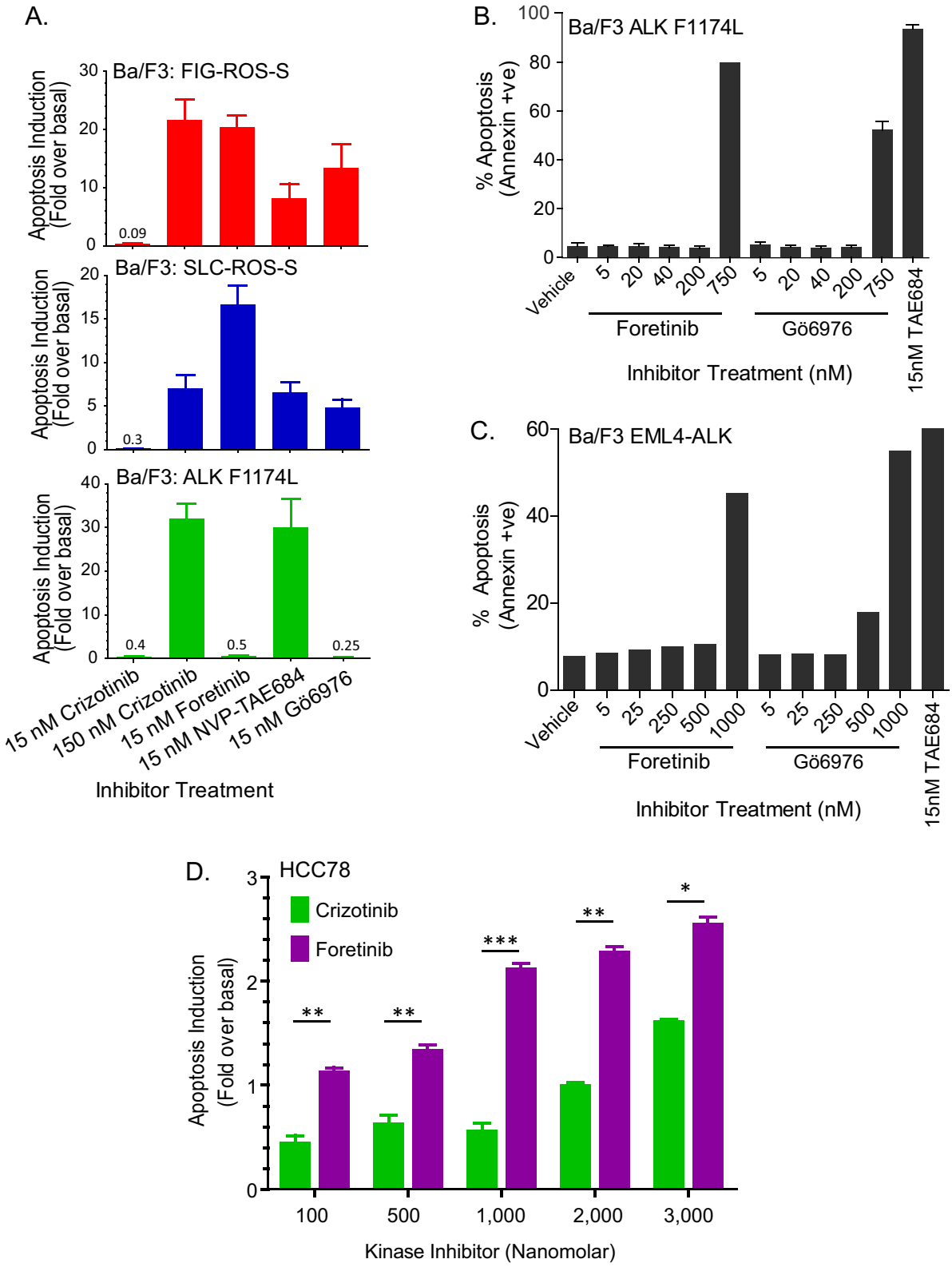

Fig. S1. Induction of apoptosis with inhibitor treatment in Ba/F3 and HCC78 cells. (*A*) Apoptosis induction in Ba/F3 FIG–ROS, SLC–ROS, and ALK^{F1174L} cells after 48 h of 15-nM inhibitor treatment as indicated. Number of cells that were Annexin V and 7-Aminoactinomycin D positive after inhibitor treatment were normalized to number of cells staining positive with these markers with vehicle treatment (basal). A minimum of 2,000 cells were counted per condition. Rate of apoptosis is shown as fold over basal. Basal apoptosis in Ba/F3 FIG–ROS, SLC–ROS, and ALK F1174 cells was 3.6%, 2.8%, and 1.2%, respectively. (*B* and *C*) Apoptosis induction (Annexin V and 7-AAD staining) in Ba/F3 ALK^{F1174L} and EML4–ALK after 48 h of inhibitor treatment as indicated in the graphs. (*D*) Apoptosis induction in HCC78 cells after treatment with foretinib and crizotinib for 72 h. Method of detection and analysis was identical to Ba/F3 cells. Basal (vehicle treated) apoptosis in HCC78 cells was 11% of total cell population. *$P < 0.05$, **$P < 0.01$ and ***$P < 0.0001$ by *t* test.

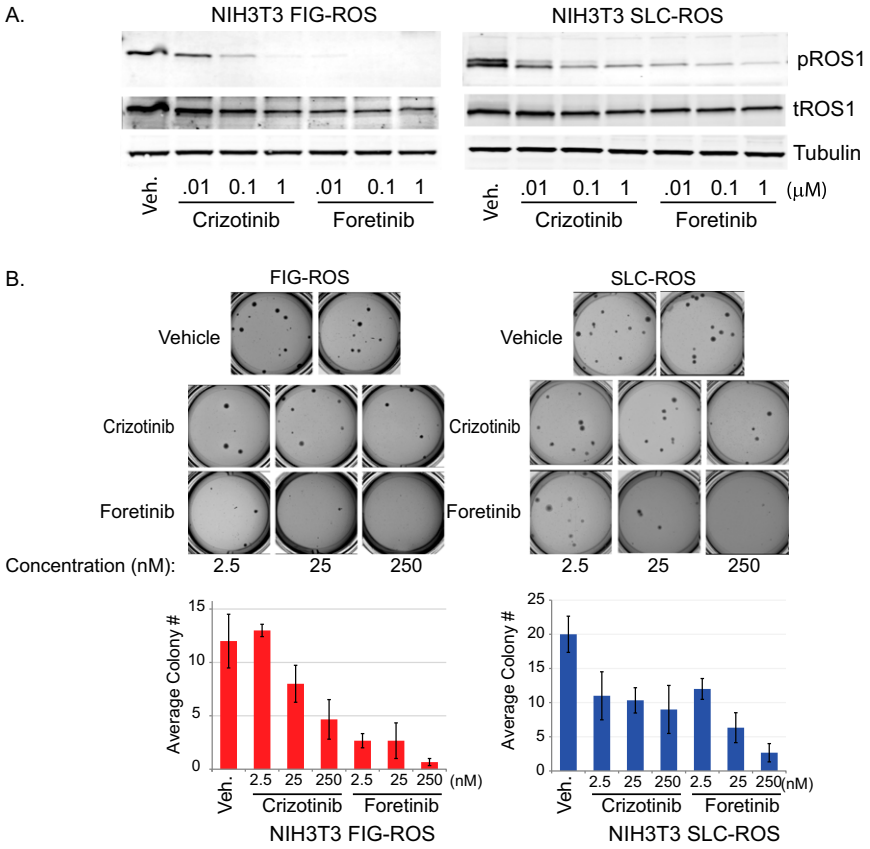

Fig. S2. Foretinib and crizotinib suppress ROS1 fusion phosphorylation and diminish anchorage-independent colony formation in transformed NIH 3T3 cells. (*A*) Immunoblot analysis of ROS1 fusion phosphorylation from NIH 3T3 FIG–ROS and SLC–ROS cells treated with varying concentrations of crizotinib and foretinib for 1 h. (*B*, *Upper*) Representative images of NIH 3T3 FIG–ROS and SLC–ROS colony formation in soft agar with and without varying dose of crizotinib and foretinib. (*Lower*) Quantification of colony number formed from vehicle or inhibitor-treated NIH 3T3 FIG–ROS and SLC–ROS cells. Graph shows average colony number ± SEM from four independent wells.

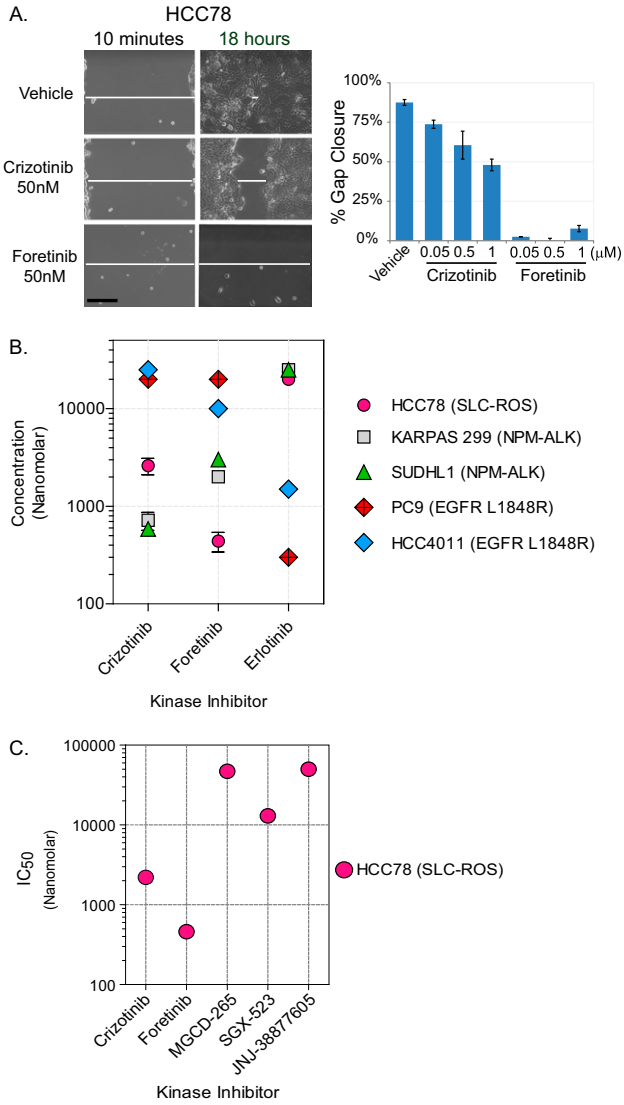

Fig. S3. Analysis of inhibitor effect on SLC-ROS expressing non-small cell lung cancer cell line HCC78 cell migration and assessment of foretinib specificity in HCC78 cells. (*A*, *Left*) Representative images show gap at 10 min and gap closure at 18 h post "scratch" after vehicle, 50 nM crizotinib, or 50 nM foretinib treatment. (*Right*) Quantification of gap closure determined by measuring micrometer length of a straight line drawn across the gap from imaging the same field of view at initiation of treatment and at 18 h (end of treatment). (Scale bar, 200 μm.) (*B*) IC_{50} values for HCC78, KARPAS 299 (lymphoma), SUDHL1 (lymphoma), PC9 (lung adenocarcinoma), and HCC4011 (lung adenocarcinoma) cells treated with crizotinib, foretinib, and erlotinib as determined from nonlinear regression curve fit analysis of the dose–response curves. (*C*) IC_{50} values for HCC78, treated with MET kinase inhibitors crizotinib, foretinib, MGCD-265, SGX-523, and JNJ-38877605 as determined from nonlinear regression curve fit analysis of the dose–response curves.

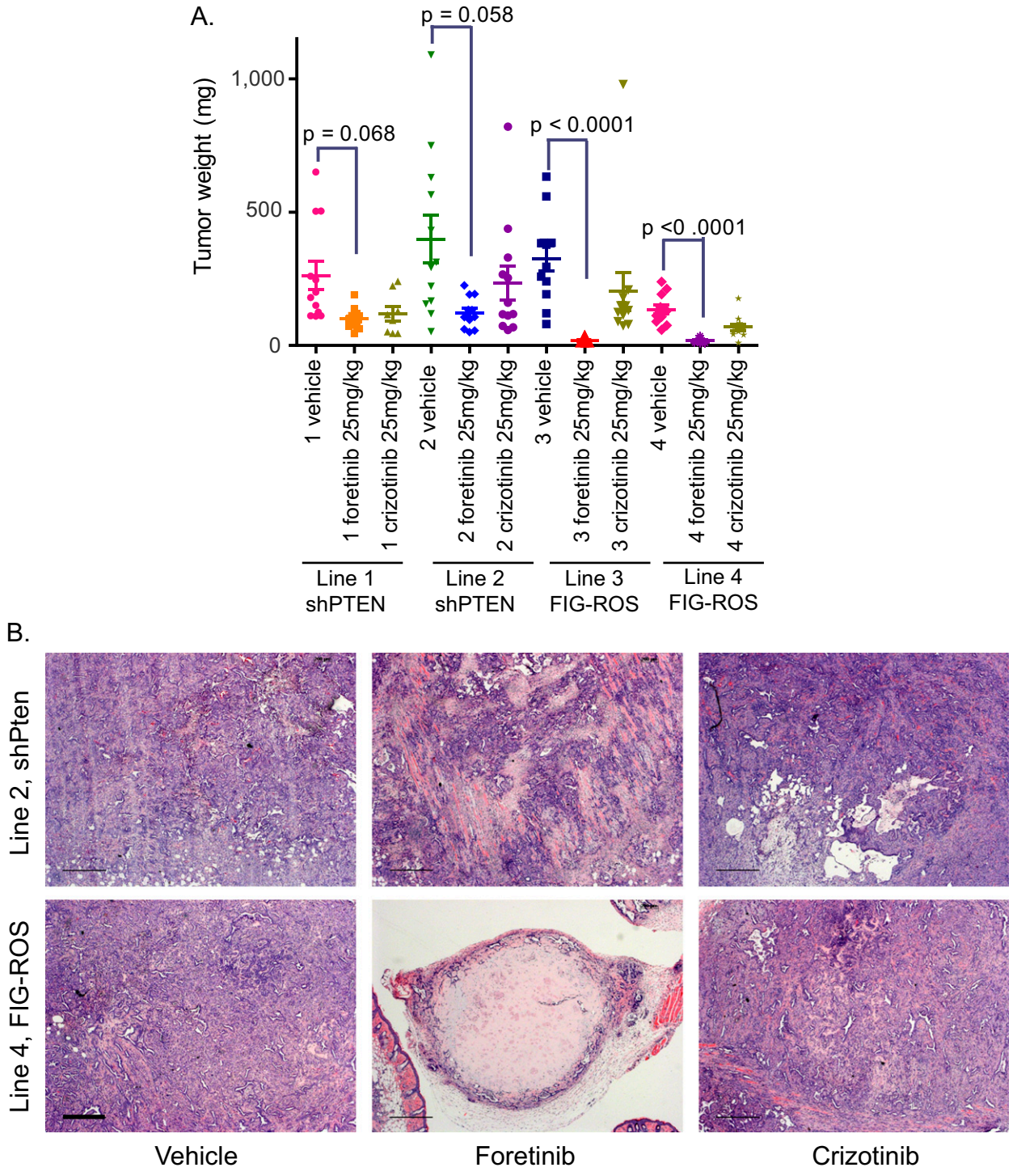

Fig. S4. Inhibitor-treated FIG–ROS and shPten tumor weight and histopathology images. (*A*) Scatter plot shows the individual weight distribution of treated tumors from lines 1 and 2 for shPten tumors and lines 3 and 4 for FIG–ROS-expressing tumors. Statistical significance determined with paired *t* test. (*B*) Representative sections of H&E stained tumors from line 2 (shPten) and line 4 (FIG–ROS) after 9 d of inhibitor treatment as indicated. (Scale bar, 500 μm.)

A.

Crizotinib (nM)	Total # of wells
500	192
750	192
1000	288
1500	384
2000	480
2500	480

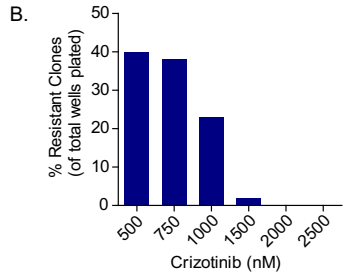

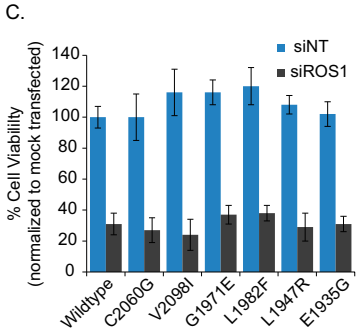

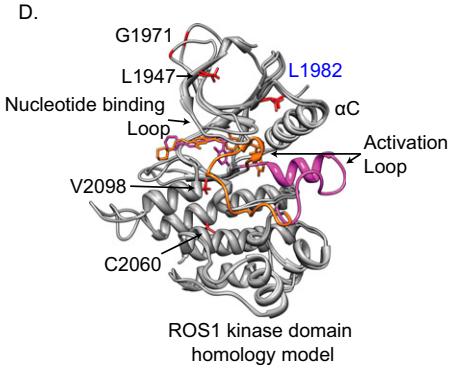

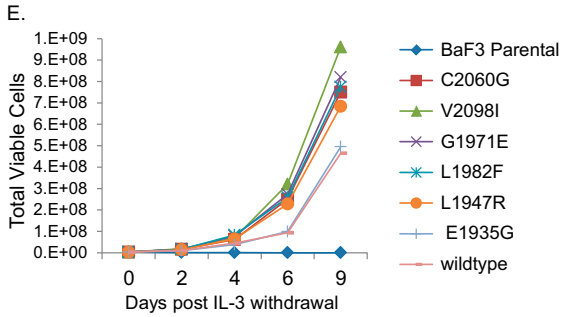

Fig. S5. Recovered Ba/F3 FIG–ROS crizotinib-resistant clones remain dependent on FIG–ROS and are independently transforming in Ba/F3 cells. (*A*) Table shows the number of wells of 96-well plates surveyed with 500; 750; 1,000; 1,500; 2,000; and 2,500 nM crizotinib after ENU-induced mutagenesis. (*B*) Number of wells with crizotinib-resistant clones for each concentration that were recovered, expressed as a percentage of the total number of wells seeded. (*C*) Viability of Ba/F3 FIG–ROS mutant cell lines recovered from ENU-mutagenesis screen after electroporation with siRNA for ROS1 kinase domain (siROS1) and nontargeting (siNT). Viability of siNT and siROS1-transfected cells was normalized to mock (sterile water)-transfected cells. (*D*) Homology model of ROS1 kinase domain bound to crizotinib (magenta) and foretinib (orange). The ligands are shown in colored stick representation, whereas the protein is shown in gray ribbon. Differences in the activation loop conformations are highlighted by coloring according to the respective ligands. Residues that were found to confer resistance to crizotinib when mutated are highlighted in red and shown as stick representations. (*E*) IL-3 withdrawal assay for Ba/F3 cells transfected with wild-type or indicated mutant FIG–ROS. Total viable cell number was determined by counting cells on days 2, 4, 6, and 9 after IL-3 withdrawal.

A.

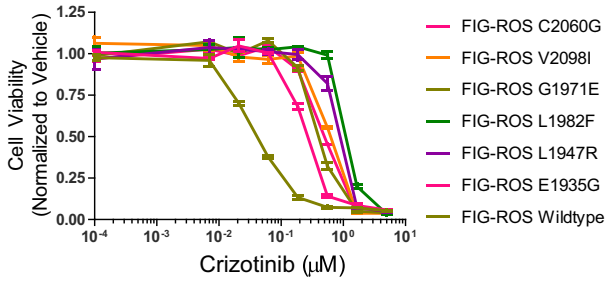

B.

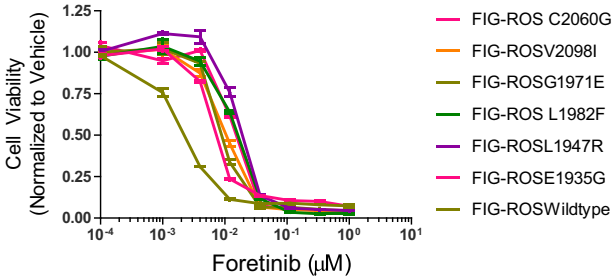

C.

Ba/F3 FIG-ROS	Crizotinib IC_{50} (nM)	Foretinib IC_{50} (nM)
Wildtype	37.5	2.03
C2060G	690	13.6
V2098I	901	9.9
G1971E	605	8.69
L1982F	2450	15.27
L1947R	1420	17.87
E1935G	350	6.6

D.

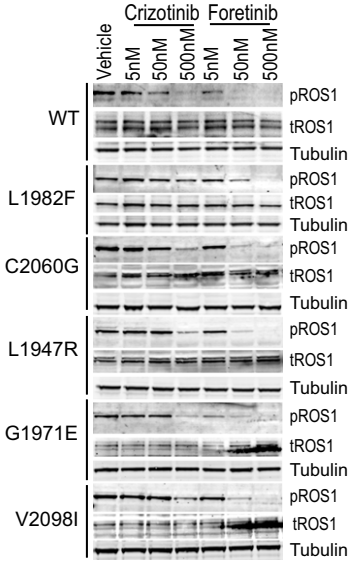

Fig. S6. Crizotinib and foretinib sensitivity of Ba/F3 FIG–ROS wild-type and kinase domain mutant-expressing transformed cells. (*A* and *B*) Dose–response curve showing growth of Ba/F3 FIG–ROS wild-type and kinase domain mutant cells after 72 h exposure with varying concentrations of crizotinib (*A*) and foretinib (*B*) as normalized to vehicle-treated cells. The values are means ± SEM from three independent experiments with triplicate wells. (*C*) Table showing IC_{50} values of crizotinib and foretinib for Ba/F3 FIG–ROS kinase domain mutants. (*D*) Immunoblot analysis of wild-type and kinase domain mutant FIG–ROS phosphorylation at varying doses of crizotinib and foretinib in Ba/F3 cells. Cropped images representative of two independent experiments are shown.

Other Supporting Information Files

Dataset S1. List of inhibitors, 384-well plate layout, and the normalized FIG–ROS cell viability data for all of the inhibitors tested in the high-throughput inhibitor platform

Dataset S1

Dataset S2. In vitro binding affinities (K_d) of a subset of kinase inhibitors for ROS1, ALK, MET, EGFR, PDGFRA, and/or IGF1R as previously reported

Dataset S2